

Control of Magnetically-Driven Screws in a Viscoelastic Medium

Zhengya Zhang[§], Anke Klingner[†], Sarthak Misra^{§*}, and Islam S. M. Khalil^{*}

Abstract—Magnetically-driven screws operating in soft-tissue environments could be used to deploy localized therapy or achieve minimally invasive interventions. In this work, we characterize the closed-loop behavior of magnetic screws in an agar gel tissue phantom using a permanent magnet-based robotic system with an open-configuration. Our closed-loop control strategy capitalizes on an analytical calculation of the swimming speed of the screw in viscoelastic fluids and the magnetic point-dipole approximation of magnetic fields. The analytical solution is based on the Stokes/Oldroyd-B equations and its predictions are compared to experimental results at different actuation frequencies of the screw. Our measurements matches the theoretical prediction of the analytical model before the step-out frequency of the screw owing to the linearity of the analytical model. We demonstrate open-loop control in two-dimensional space, and point-to-point closed-loop motion control of the screw (length and diameter of 6 mm and 2 mm, respectively) with maximum positioning error of 1.8 mm.

I. INTRODUCTION

There have been many successful biologically-inspired approaches to provide locomotion at low Reynolds number (Re) regime. Swimming using helical propulsion based on the *Escherichia coli* bacteria has been achieved by Bell *et al.* and Ghosh *et al.* using homogenous magnetic fields [1], [2]. These magnetic fields exert magnetic torque on the dipole of the helical microrobots, and hence allow them to rotate and move through screw-based motion in fluids and tissue [3]. The wireless control in fluidic environment, micrometer-level precision, and the small size of these microrobot make them viable for diverse clinical applications [4]-[8]. With helical propulsion, even so more than with other actuation techniques, the microrobot has the ability to swim under a wide range of Re in the range of 0.01 to 1000. In addition, helical propulsion enables microrobots to swim in viscous fluids and drill through complex viscoelastic media. Therefore, they could potentially perform tasks in biological fluids and tissue.

Nelson *et al.* have developed an empirical model of magnetically-driven screws to predict the role of magnetic, rheological, and actuation parameters on the turning radius

[§]Surgical Robotics Laboratory, Department of Biomedical Engineering, University of Groningen and University Medical Center Groningen, Groningen, The Netherlands.

[†]Physics Department, The German University in Cairo, Cairo, Egypt.

^{*}Surgical Robotics Laboratory, Department of Biomechanical Engineering, Faculty of Engineering Technology, University of Twente, Enschede, The Netherlands.

This research has received funding from the European Research Council (ERC) under the European Union's Horizon 2020 Research and Innovation programme (Grant Agreement 638428 - project ROBOTAR), and the financial support of China Scholarship Council (CSC).

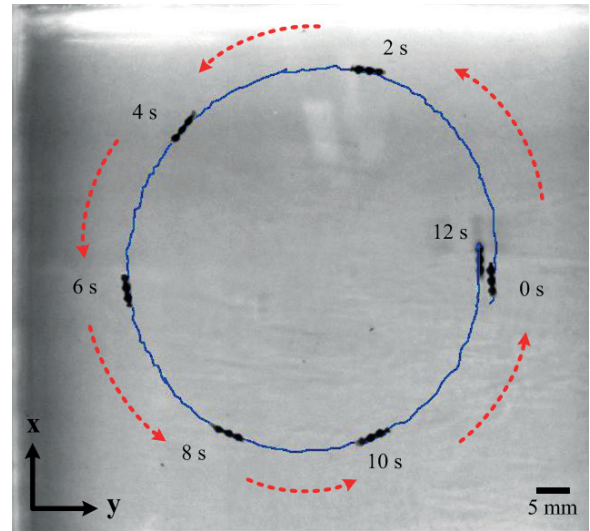


Fig. 1. A magnetically-driven screw is moved controllably in soft-tissue phantom (0.8 wt.% agar gel) along a circular trajectory. The screw is actuated by two rotating dipole fields and swims at an average speed of 15 mm/s. The blue trajectory and the curved red arrows indicate the path and direction of the screw, respectively. Please refer to the accompanying video.

of the screw [9]. Schamel *et al.* have demonstrated that nanoscrews move controllably through high-viscosity solutions [10]. They have also observed propulsion enhancement that exceeds the highest measured speeds in Newtonian fluids for heterogenous gel-like media with a mesh size larger than the swimmer size. Walker *et al.* have developed magnetic micropropellers that mimic bacteria in swimming through mucus by producing the enzyme urease to raise the pH locally and dissolve the mucus [11]. Wu *et al.* have also developed intravitreal delivery micropropellers that can be actively propelled through the vitreous humor to reach the retina [12]. Recently, Xu *et al.* have also demonstrated image-based visual servoing of helical microswimmers and arbitrary path following in two dimensions [13], [14]. These microrobots are typically actuated using uniform magnetic fields produced by orthogonal arrangements of electromagnetic coils with a limited projection distance.

In contrast to actuation with orthogonal arrangement of coils, Fountain *et al.* [15] and Mahoney *et al.* [16], [17] have demonstrated helical propulsion using non-uniform magnetic fields produced by a single rotating permanent magnet. The rotating permanent magnet is positioned with a 6-DOF robotic manipulator to enable actuation over relatively large workspace compared to orthogonal arrangements of electromagnetic coils. Ryan and Diller have also presented

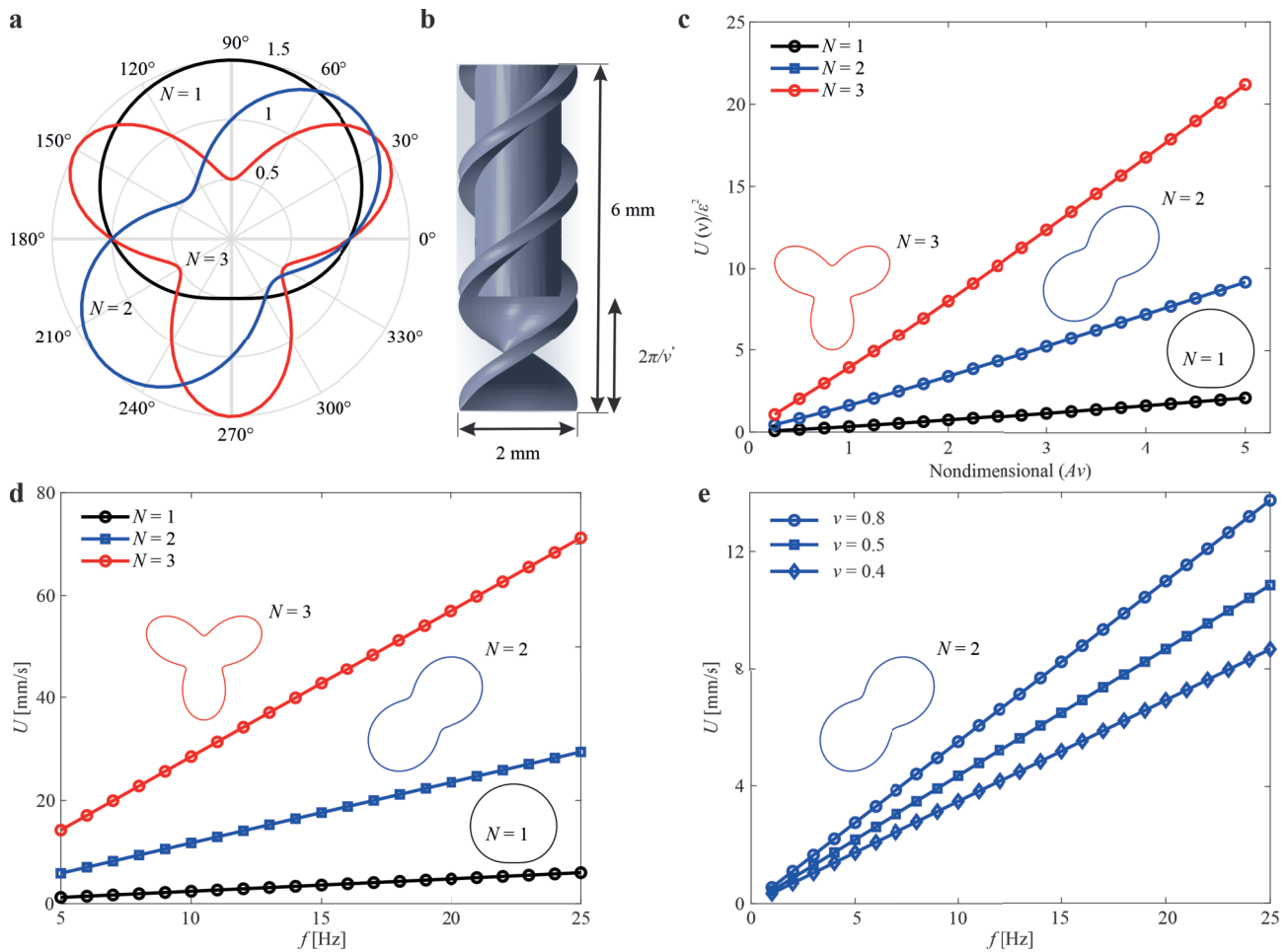


Fig. 2. The profile of the screw influences its swimming speed in a viscoelastic medium. (a) Three representative screw profiles (ρ) are calculated using $\rho(\theta) = 1 + \epsilon \sin(N\theta)$, for $\epsilon = 0.5$, $N = 1 : 3$, and $\theta \in [0, 2\pi)$. N is the number of starts of the screw. (b) The permanent magnet with magnetization direction orthogonal to the long axis of the screw is fixed inside the cylinder (with radius A). (c) Swimming speed of the screw is calculated as function of ν for $N = 1, 2, 3$. (d) The swimming speed (U) of the screw increases with the number of starts and the actuation frequency (f). (e) U increases with f and ν for $N = 2$, and $\epsilon = 0.33$. The swimming velocity is calculated using equation (4).

a permanent magnet-based actuation system consisting of eight permanent magnets [18]. The eight permanent magnets can create fields and field gradients in any direction with variable magnitudes to achieve feedback control of microagents. It has also been demonstrated that the attractive forces acting on the microrobot can be converted into a lateral force using an open-loop trajectory by Mahoney *et al.* [19]. Alshafei *et al.* [20] and Hosney *et al.* [7], [21] have also shown that the attractive forces along the lateral direction of the microrobot can be eliminated by using two synchronized rotating dipole fields and open-loop control has been demonstrated inside a viscous medium to clear clogged vessels.

In this work we study the closed-loop behaviour of magnetically-driven screws in viscoelastic medium (agar gel) under the influence of non-uniform rotating dipole fields (Fig. 1). A closed-loop control system is developed based on an analytical solution of the swimming speed of the screw and the magnetic point-dipole approximation of the magnetic fields, and we achieve the following: (1) Implement an analytical solution based on the Stokes/Oldroyd-B

equations to predict the swimming speed of the screw [22], [23]; (2) Characterization of the frequency response of magnetically-driven screws and comparison between measurements and analytical results; (3) Open- and closed-loop control in agar gel.

The remainder of this paper is organized as follows: In Section II, an analytical solution of the swimming speed of the magnetically-driven screw in viscoelastic fluids is used in the development of a closed-loop control system. Section III provides descriptions of our permanent magnet-based robotic system, characterization of the frequency response of the screw and comparison with the theoretical predictions of the Stokes/Oldroyd-B equations, and open- and closed-loop control results. Finally, Section IV concludes and provides directions for our future work.

II. MODELING AND CONTROL OF MAGNETICALLY-DRIVEN SCREWS

Magnetically-driven screws are immersed in low- Re medium and actuated using non-uniform magnetic field.

A. Magnetically-Driven Screws

We consider a screw with magnetic dipole moment \mathbf{m} perpendicular to its helix axis, consisting of a helical wave superimposed onto a cylinder of radius A . Its surface is described by [22], [23]

$$\mathbf{x}(\theta, \zeta) = A\rho(\theta)[\cos(v^*\zeta + \theta)\hat{\mathbf{x}} + \sin(v^*\zeta + \theta)\hat{\mathbf{y}}] + \zeta\hat{\mathbf{z}}, \quad (1)$$

where θ and ζ are helical coordinates such that $\theta \in [0, 2\pi)$ and $\zeta \in (-\infty, \infty)$. Further, the helical pitch is $2\pi/v^*$ and the pitch angle is given by $\gamma = \tan^{-1}(v^*A)$. The function $\rho(\theta) = 1 + \varepsilon f(N\theta)$ indicates the profile of the cross-section of the screw, where $f(N\theta)$ is a periodic function and N is the number of starts of the screw. Fig. 2(a) shows different profiles for the screw. The screw (Fig. 2(b)) is subject to a magnetic torque $\boldsymbol{\tau} = \mathbf{m} \times (\mathbf{B}_1 + \mathbf{B}_2)$ exerted by two rotating dipole fields \mathbf{B}_1 and \mathbf{B}_2 . These fields are generated by two rotating permanent magnets and modeled with the following point-dipole approximation [15]-[17]:

$$\mathbf{B}_i(\mathbf{p}) = \frac{\mu_0}{4\pi |\mathbf{p}|^3} \left(\frac{3(\mathbf{M}_i \cdot \mathbf{p})\mathbf{p}}{\mathbf{p}} - \mathbf{M}_i \right) \text{ for } i = 1, 2, \quad (2)$$

where μ_0 is the permeability of free space and \mathbf{p} is the position vector of the screw with respect to the rotating permanent magnet. Further, \mathbf{M}_i is the magnetic dipole moment of the i th permanent magnet. Because \mathbf{M} rotates at a controlled constant angular velocity (results in translation speed as shown in Fig. 3(a)), \mathbf{M} is constructed using \mathbf{q} as

$${}^0\mathbf{T}_i^3(\mathbf{q}) = \begin{pmatrix} {}^0\mathbf{R}_i^3 & {}^0\mathbf{p}_i^3 \\ \mathbf{0}_{1 \times 3} & 1 \end{pmatrix} \text{ for } i = 1, 2, \quad (3)$$

where ${}^0\mathbf{T}_i^3(\mathbf{q})$ is the i th homogenous transformation matrix from the frame of reference of the i th permanent magnet to a reference frame and $\mathbf{q} = (\phi, \alpha, \beta)^T$ is a vector of the joint space coordinates. Further, ${}^0\mathbf{R}_i^3$ and ${}^0\mathbf{p}_i^3$ are the rotation matrix and position vector of the i th permanent magnet with respect to a frame of reference (Fig. 3(b)), respectively. The orientation of the actuating magnets is described using equation (3) and \mathbf{M} is constructed using \mathbf{q} .

B. Swimming Speed in Viscoelastic Fluid

The magnetic torque rotates the screw at angular speed ω and the following linear speed U [22], [23]:

$$U = 2A\omega\varepsilon^2 \sum_{q \geq 1} \frac{(1 + \beta q^2 De^2) |\hat{f}_q|^2}{1 + q^2 De^2} J_q, \quad (4)$$

where De is the Deborah number and given by

$$De = \lambda\omega, \quad (5)$$

where λ is the fluid relaxation timescale. Further, β is the ratio of the solvent viscosity to the total viscosity of the solution and polymer ($\beta = \eta_s/\eta$). In (4), \hat{f}_q is Fourier analysis of the periodic function $f(N\theta)$ and the function J_q is calculated based on Bessel function K_x at $x = qv$, where v is the normalized pitch $v = v^*A$

$$J_q = \frac{q^2 A_q}{2} \left(2K_{q-1} - vK_q + \frac{vK_{q-1}^2}{K_q} \right), \quad (6)$$

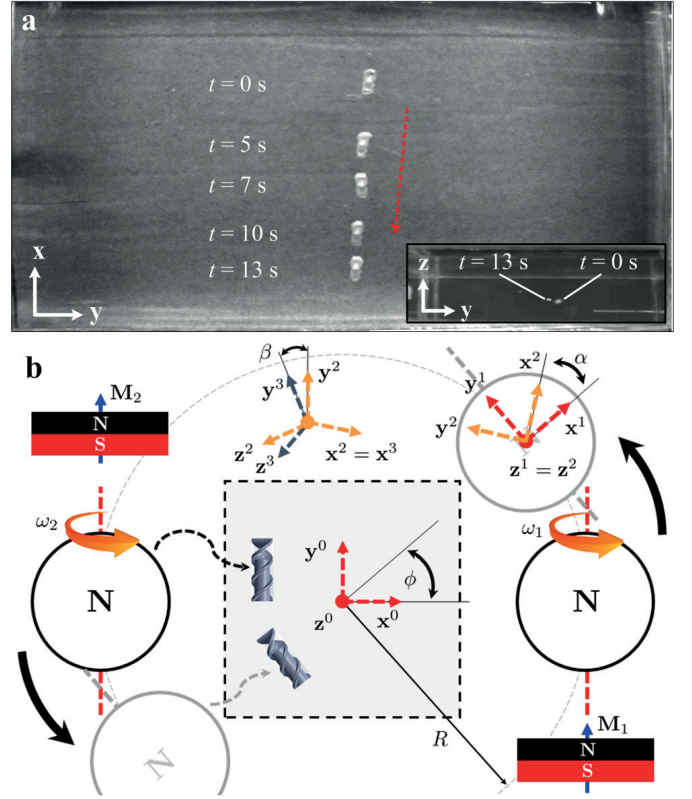


Fig. 3. A magnetically-driven screw is moved controllably in soft-tissue phantom. (a) The screw is actuated by two rotating permanent magnets with magnetic moment (M) at angular speed ($\omega_1 = \omega_2$). (b) The pitch (β) and steering (α) angles of the permanent magnets enable the screw to rotate and achieve out of plane swim. The two permanent magnets are also rotated with respect to a reference frame of reference with angle ϕ . \mathbf{M}_1 and \mathbf{M}_2 are the magnetization vectors of the permanent magnets and reside along their long axes. The dashed square indicates the workspace (105 mm \times 105 mm \times 40 mm) of the system.

where the constants A_q are calculated using

$$A_q = \frac{2 \left(q + \frac{qvK_{q-1}}{K_q} \right)}{qK_q + qvK_{q-1} - \Lambda_q}, \quad (7)$$

$$\Lambda_q = \frac{2(q-2)}{v} K_{q-1} + \frac{(3q-2)K_{q-1}^2}{K_q} + \frac{qvK_{q-1}^3}{K_q^2}.$$

Equation (4) predicts the swimming speed of the helix based on the characteristics of the viscoelastic medium, parameters of the screw, and the angular speed of the screw. Fig. 2(c) shows the calculated swimming speed of the screw as function of the helical pitch ($2\pi/v$) for three representative values of number of starts (N). The swimming speed increases with v and N , at actuation frequency of 5 Hz. The swimming speed of the screw also depends on the actuation frequency. Figs. 2(d) and 2(e) show the calculated swimming speed of the screw at actuation frequency of $f \in [5, 25]$ Hz and for three representative screw profiles, $f(\theta) = 1 + 0.5 \sin(N\theta)$ for $N = 1 : 3$ and $\theta \in [0, 2\pi)$ and three representative helical pitches. The calculated speed of the screw increases with the actuation frequency and the number of starts of the screw profile.

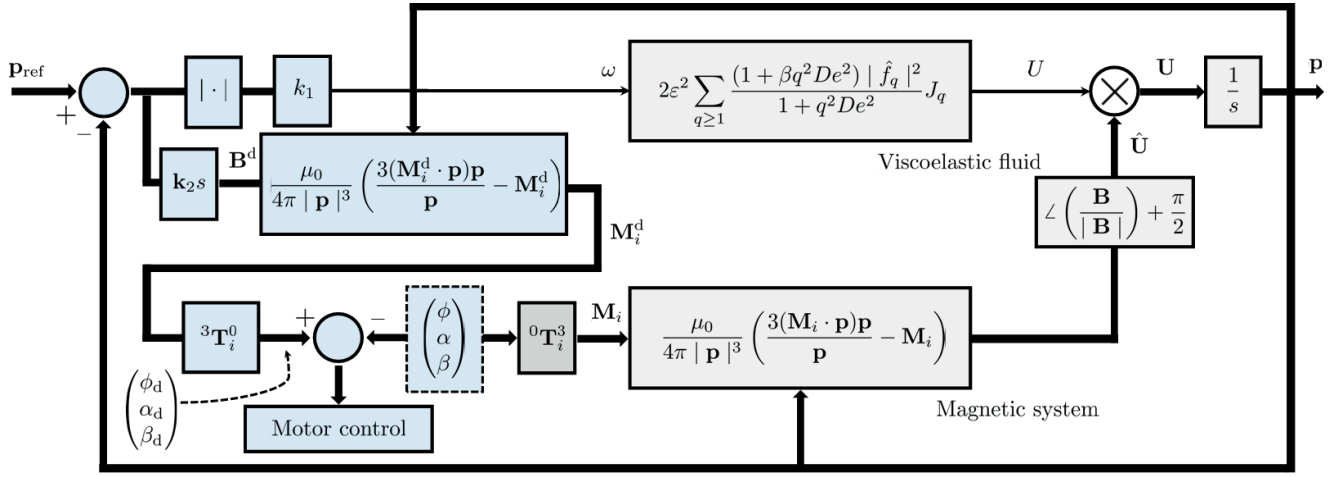


Fig. 4. Closed-loop control of magnetically-driven screws is achieved based on an analytical solution of the swimming speed and the point-dipole model of the magnetic fields. The control inputs are the angular speed (ω) and the orientation of the magnetization vector (\mathbf{M}). The nominal parameters of the screw and viscoelastic fluid are used to calculate the variable (ϵ), viscosity ratio (β), Deborah number (De), and the function J_q .

C. Control System Design

We assume that the external magnetic field and the magnetic dipole provide enough torque and the helix axis of the screw ultimately align with the magnetic field lines. Therefore, the direction of the screw is calculated based on the direction of the magnetic field at the position of the screw and this assumption yields

$$\angle \mathbf{m} = \angle \mathbf{B}(\mathbf{p}) \Rightarrow \angle \mathbf{U} = \angle \mathbf{m} + \frac{\pi}{2}. \quad (8)$$

We also assume that the dipole fields are rotating below a step-out frequency (ω_{so}) of the screw. This step-out frequency limits the frequency response as the screw does not remain synchronized with the external magnetic fields. Therefore, the angular velocity of the rotating dipole fields are calculated using

$$\omega = \begin{cases} k_1 |\mathbf{p}_{ref} - \mathbf{p}|, & \omega < \omega_{so} \\ \kappa \omega_{so}, & \omega \geq \omega_{so} \end{cases} \quad (9)$$

where k_1 is a positive gain and $0 < \kappa < 1$. The control input (9) provides zero output for zero position tracking error $|\mathbf{p}_{ref} - \mathbf{p}|$, thereby decreasing the linear speed of the screw as it approaches the reference position. The second control input is the direction of the magnetic field. This direction is controlled by the magnetization vectors of the rotating permanent magnets \mathbf{M}_i . The point-dipole model (2) is provided with the desired magnetic fields based on the orientation error of the screw. Therefore, the desired orientation of the magnetic field is calculated using

$$\angle \mathbf{B}(\mathbf{p}) = \tan^{-1} \left(\frac{|\mathbf{p}_{ref} - \mathbf{p}|_y}{|\mathbf{p}_{ref} - \mathbf{p}|_x} \right), \quad (10)$$

where $|\mathbf{p}_{ref} - \mathbf{p}|_{x,y}$ is the position error along x - and y -axis, respectively. The angle of the desired magnetic field $\angle \mathbf{B}(\mathbf{p})$ and its unit vector $\hat{\mathbf{B}}(\mathbf{p})$ are used to construct $\mathbf{B}(\mathbf{p})$ and calculate \mathbf{M}_i using (2). This calculation is done by setting $\mathbf{m} \times \mathbf{B}^d \Rightarrow \mathbf{k}_2(\dot{\mathbf{p}}_{ref} - \dot{\mathbf{p}})$ to calculate the desired magnetic

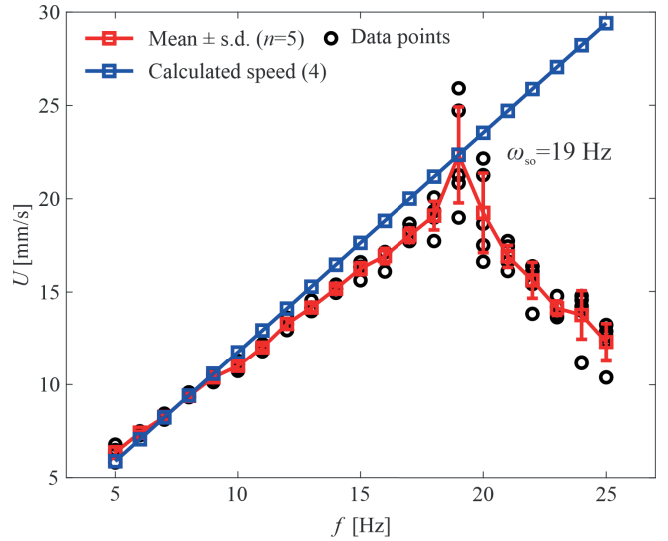


Fig. 5. Frequency response of a 6-mm-long screw is characterized in 0.8 wt.% agar gel. The screw is allowed to swim within the center of two rotating dipole fields inside a gelatin reservoir. The distance between the two rotating dipole fields is 21 cm, and the magnitude of the magnetic field at the position of the screw is 47 mT. The step-out (ω_{so}) of the screw is 19 Hz at magnetic field of 10 mT. Each data point represents the average swimming speed U of five trials at each actuation frequency f .

field \mathbf{B}^d , where \mathbf{k}_2 is a positive-definite matrix. Fig. 4 shows the implementation of the control system.

III. CLOSED-LOOP MOTION CONTROL

Control of the screw is achieved using a permanent magnet-based robotic system inside agar gel tissue phantom.

A. System Description

The magnetic control of the screw is done using two synchronized rotating dipole fields. Two permanent magnets (NdFeB) with axial magnetization are fixed to DC motors to generate rotating magnetic fields. The permanent magnets (R750F, Amazing Magnets LLC, California, U.S.A) with

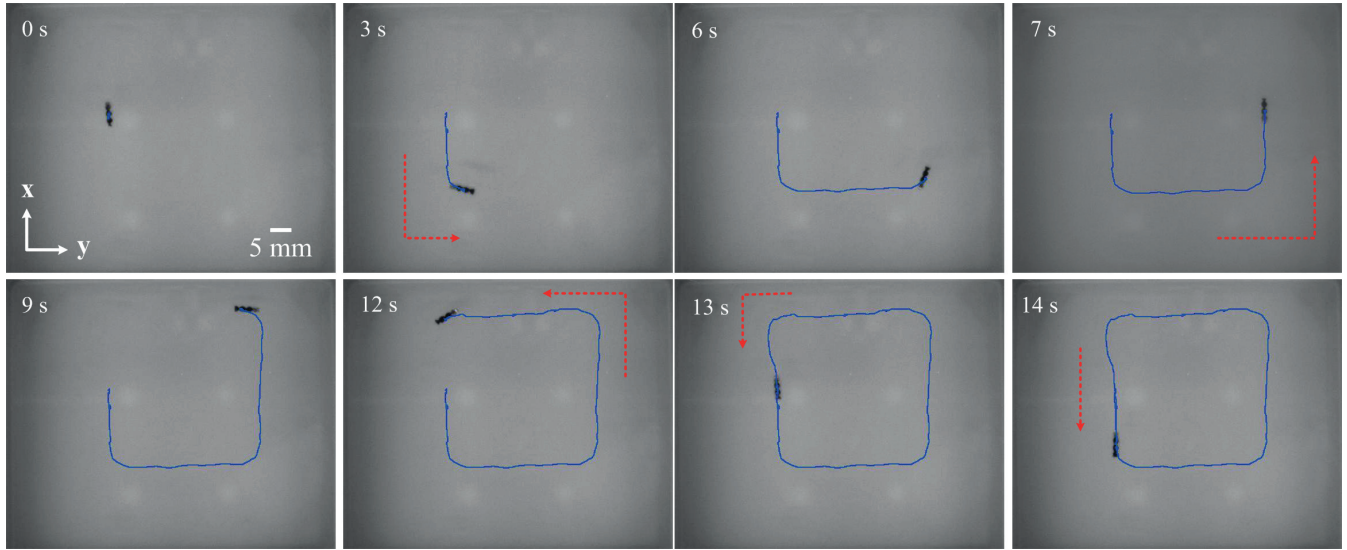


Fig. 6. Open-loop control of a magnetically-guided screw is achieved along a square trajectory with edge length of 36 mm. The screw swims at an average speed of 18 mm/s under the influence of rotating magnetic field at frequency of 2 Hz in 0.8 wt.% agar gel. The red arrow indicates the swimming direction of the screw. Please refer to the accompanying video.

diameter and height of 40 mm and 20 mm, have a magnetization of 1.72×10^{-4} A.m². The orientation of the DC motors are controlled independently to change the pitch and steering angles of the screws, as shown in Fig. 3. These angles are controlled independently to control the orientation of the screw. Each of these configurations are fixed to a rotational motion stage with radius R (rotates with angle ϕ) and the screw is allowed to swim between the rotating dipole fields.

The screw is contained inside a reservoir (105 mm × 105 mm × 40 mm) made of acrylic and is controlled to swim within the center of the two rotating dipole fields. Its position and orientation are measured by two cameras (Aviator GIGE, avA1000-100gm, Basler AG, Ahrensburg, Germany) mounted above and in front of the reservoir. The length and diameter of the screw are 6 mm and 2 mm, respectively. The helix angle and the pitch are 45° and 2 mm, respectively. The screws are 3D printed using photopolymer resin (FLGPBK04, formlabs, Somerville, USA). A cylindrical permanent magnet with diameter of 1 mm and length of 1 mm is fixed to the screw to provide a magnetic dipole moment along its radial direction. The configuration of the permanent magnets yields the following homogenous transformation:

$${}^0\mathbf{T}_i^3 = \begin{pmatrix} c\phi c\alpha_i - s\phi s\alpha_i & a_i c\beta_i & -b_i s\beta_i & Rc\phi \\ s\phi c\alpha_i + c\phi s\alpha_i & c_i c\beta_i & d_i s\beta_i & Rs\phi \\ 0 & s\beta_i & c\beta_i & 0 \\ 0 & 0 & 0 & 1 \end{pmatrix}, \quad (11)$$

where $a_i = -c\phi s\alpha_i - s\phi c\alpha_i$, $b_i = -c\phi s\alpha_i - s\phi c\alpha_i$, $c_i = -s\phi s\alpha_i + c\phi c\alpha_i$, and $d_i = s\phi s\alpha_i + c\phi c\alpha_i$. This homogenous transformation is used to determine the desired angles of the actuating magnets based on the desired magnetization \mathbf{M}^d .

Frequency response and motion control experiments are done inside agar gel. Demineralized water and gelatine

powder (Ec Nnr: 232-554-6, Boom BV, Rabroekenweg, The Netherlands) with density of 0.68 g/ml are used to prepare the agar gel in three steps. The first step is heating until the gelatine powder dissolves at 70°. The second step is dilution to a concentration of 0.8 wt.% agar gel. Finally, the mixture is cooled for 12 hours and then cut and inserted in the reservoir.

B. Frequency Response Characterization

The swimming speed of the screw is measured against the actuation frequency of the rotating dipole fields. The minimum and maximum magnitudes of the magnetic field at the position of the screw are 47 mT and 80 mT, respectively. The frequency response of the screw is shown in Fig. 5. Each data point represents the average swimming speed of five trials at each actuation frequency. The frequency response indicates that the screw does not follow the magnetic field lines above actuation frequency of 19 Hz. Therefore, the step-out frequency of the screw is 19 Hz. At this frequency, the swimming speed is measured as 22.3 ± 2 mm/s. The frequency response of the screw indicates that the analytical solution of the Stokes/Oldroyd-B equations is in agreement with the measurements below the step-out frequency. Therefore, equation (4) is incorporated into the closed-loop control system and the actuation frequency is limited below 19 Hz.

C. Open-Loop Control Results

Fig. 1 shows superimposed still images demonstrating open-loop control of the screw. In this experiment, the steering and pitch angles of the permanent magnets are fixed and only the angular velocity of the rotating motion stage is set to a constant speed. The permanent magnets are synchronized and allowed to rotate at an angular frequency of 4 Hz. This control enables the screw to swim along a circular trajectory and the swimming speed is measured as 15 mm/s. This result indicates that the screw can swim controllably

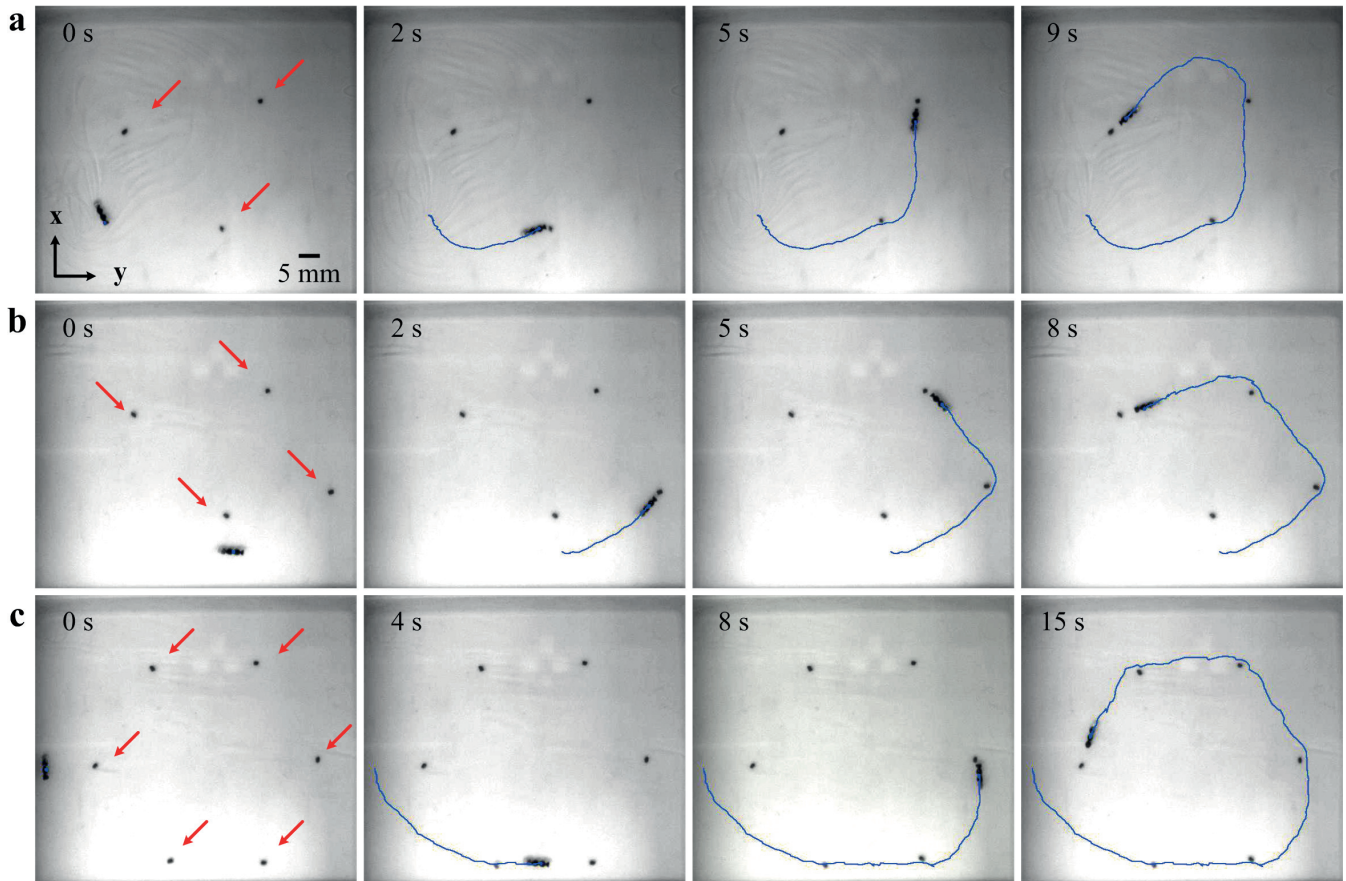


Fig. 7. A magnetically-driven screw swims controllably toward reference positions (indicated by the red arrows) under the influence of controlled magnetic fields in 0.8 wt.% agar gel. (a) The screw swims toward three reference positions with maximum position error of 1.25 mm. (b) The screw swims toward four reference positions with maximum position error of 1.82 mm. (c) The screw swims toward six target positions in a hexagon configuration with maximum position error of 1.69 mm. *Please refer to the accompanying video.*

using single degree of freedom (ϕ) of the permanent magnet-based robotic system. Another representative open-loop trial is shown in Fig. 6. In this case, the screw is controlled to swim along a square trajectory with edge length of 36 mm at an average speed of 18 mm/s. Similarly to the circular trajectory, the angle ϕ is used to control the screw. In both examples, the magnets are synchronized and the motion of the rotational stage is controlled based on the prescribed trajectory. In practice, the pitch and steering angles of the screw have to be controlled toward the reference position. *Please refer to the accompanying video.*

D. Point-to-Point Closed-Loop Control Results

Fig. 7(a) shows a representative closed-loop control trial of the screw toward three target positions. Small particles (red arrows) are added into the agar gel and used as targets for the screw. The targets are positioned at random locations and separated with approximately 5-6 body length. In contrast to the previous open-loop control experiments, the position and orientation of the screw and the position of the targets are used in (9) and (10) to calculate the control inputs ω and $\angle \mathbf{B}(\mathbf{p})$. This angle is used to construct the desired direction of the magnetization vector of the actuating magnet using

the point-dipole approximation of the field (2). Finally, the desired angles of the permanent magnet-based robotic system are calculated based on the homogenous transformation (11) and the desired magnetization vector \mathbf{M}^d .

The desired angles (ϕ , α , and β) are controlled and updated based on the reference position. In the case of Fig. 7(a), the screw swims controllably toward three targets with maximum position error of 1.25 mm. At $t = 5$ second, the screw swim toward the prescribed location and at rotates to move toward the last prescribed location ($t = 9$ second). This trial indicates that the curvature of the trajectory is relatively large. Similarly to Fig. 7(a), four markers (targets) are randomly inserted inside the agar gel and the screw achieves point-to-point control with maximum position error of 1.82 mm. In Fig. 7, six particles are inserted in a hexagon configuration and the screw achieves closed-loop control with maximum position error of 1.69 mm. *Please refer to the accompanying video.*

The positioning error of the closed-loop control trials depends on the prescribed locations of the targets. Relatively small positioning error is observed when the targets are located in the swimming direction of the screw. In this case, the screw changes its orientation while swimming

in the same direction, as shown in Fig. 7(c) at $t = 4$ second. The positioning error increases when the swimming direction of the screw is altered, as shown in Fig. 7(b) and Fig. 7(c) at $t = 15$ and $t = 5$ second, respectively. The turning curvature of the screw depends on its swimming velocity, magnetic moment and magnetic field, geometry, and properties of the agar gel [9]. Therefore, it is possible to enhance the performance of the closed-loop control system by decreasing the turning curvature of the screw using the swimming speed during experimental runs. It is also possible to exert greater magnetic torque and decrease the turning radius by incorporating permanent magnets with relatively large magnetic moment during fabrication.

IV. CONCLUSIONS AND FUTURE WORK

Open- and closed-loop motion control of magnetically-driven screws are achieved using a permanent magnet-based robotic system in agar gel tissue phantom. The frequency response of the screw is characterized and good match is observed between measurements and calculated speeds based on an analytical solution of the Stokes/Oldroyd-B equations. The analytical solution and measurements are in agreement below the step-out frequency of the screw. In the case of open-loop control, we demonstrate the ability to swim along simple trajectories using single degree of freedom of the system. In the case of closed-loop control, the screw is controlled toward arbitrary targets with maximum position error of 1.82 mm.

As part of future studies, the magnetically-driven screw will be tested in real tissue and bodily fluids. This *ex vivo* study is essential to test the capability of our permanent magnet-based robotic system to actuate the screw in conditions encountered *in vivo* such as the time-varying flow rates, heterogenous and fibrous environments. The screw will also be fabricated using biodegradable polymer and drug will be incorporated into its polymer matrix to deploy localized therapy in soft-tissue environment. In addition, the Stokes/Oldroyd-B equations will be compared to screws with different geometries (diameter, length, helical pitch, rim depth), different magnetic properties (magnetic moment and magnetic field), inside fluids with different rheological properties (viscosities), and near to a solid boundary. This comparison is essential to predict the speed of a wide range of magnetically-driven screws in different conditions.

REFERENCES

- [1] D. J. Bell, S. Leutenegger, K. M. Hammar, L. X. Dong, B. J. Nelson, "Flagella-like propulsion for microrobots using a magnetic nanocoil and a rotating electromagnetic field", in *Proceedings of the IEEE International Conference on Robotics and Automation (ICRA)*, pp. 1128-1133, April 2007.
- [2] A. Ghosh and P. Fischer, "Controlled propulsion of artificial magnetic nanostructured propellers" *Nano Letters*, vol. 9, no. 6, pp. 2243-2245, May 2009.
- [3] K. Ishiyama, K. I. Arai, M. Sendoh, and A. Yamazaki, "Spiral-type micro-machine for medical applications," *Journal of Micromechatronics*, vol. 2, no. 1, pp. 77-86, April 2002.
- [4] B. J. Nelson, I. K. Kaliakatsos, and J. J. Abbott, "Microrobots for minimally invasive medicine," *Annual Review of Biomedical Engineering*, vol. 12, pp. 55-85, April 2010.
- [5] J. J. Abbott, Z. Nagy, F. Beyeler, and B. J. Nelson: Robotics in the small, part I: microbotics. *IEEE Robotics and Automation Magazine*, 14(2), pp. 92-103, 2007.
- [6] J. Wang and W. Gao, "Nano/Microscale Motors: Biomedical Opportunities and Challenges," *ACS Nano*, vol. 6, no. 7, pp. 5745-5751, July 2012.
- [7] A. Hosney, J. Abdalla, I. S. Amin, N. Hamdi, and I. S. M. Khalil, "In vitro validation of clearing clogged vessels using microrobots," in *Proceedings of the IEEE RAS/EMBS International Conference on Biomedical Robotics and Biomechanics (BioRob)*, pp. 272-277, Singapore, June 2016.
- [8] L. Dong and B. J. Nelson: Tutorial - Robotics in the small part II: nanorobotics. *IEEE Robotics and Automation Magazine*, vol. 14, no. 3, pp. 111-121, 2007.
- [9] N. D. Nelson, J. Delacenserie, and J. J. Abbott, "An empirical study of the role of magnetic, geometric, and tissue properties on the turning radius of magnetically driven screws," in *Proceedings of the IEEE International Conference on Robotics and Automation (ICRA)*, pp. 5352-5357, Karlsruhe, Germany, May 2013.
- [10] D. Schamel, A. G. Mark, J. G. Gibbs, C. Miksch, K. I. Morozov, A. M. Leshansky, and P. Fischer, "Nanopropellers and their actuation in complex viscoelastic media," *ACS Nano*, vol. 8, no. 9, pp. 8794-8801, June 2014.
- [11] D. Walker, B. T. Käsdorf, H.-H. Jeong, O. Lieleg, P. Fischer, "Enzymatically active biomimetic micropropellers for the penetration of mucin gels," *Science Advances*, vol. 1, no. 11 (e1500501), December 2015.
- [12] Z. Wu, J. Troll, H. Jeong, Q. Wei, M. Stang, F. Ziemssen, Z. Wang, M. Dong, S. Schnichels, T. Qiu, and P. Fischer, "A swarm of slippery micropropellers penetrates the vitreous body of the eye," *Science Advances*, vol. 4, no. 11 (eaat4388), November 2018.
- [13] C. Huang, T. Xu, J. Liu, L. Manamanchaiyaporn, and X. Wu, "Visual servoing of miniature magnetic film swimming robots for 3-D arbitrary path following," *IEEE Robotics and Automation Letters*, vol. 4, no. 4, pp. 4185-4191, October 2019.
- [14] T. Xu, Y. Guan, J. Liu, and X. Wu, "Image-Based visual servoing of helical microswimmers for planar path following," *IEEE Transactions on Automation Science and Engineering*, vol. 17, no. 1, pp. 325-333, January 2020.
- [15] T. W. R. Fountain, P. V. Kailat, and J. J. Abbott, "Wireless control of magnetic helical microrobots using a rotating-permanent-magnet manipulator," in *Proceedings of the IEEE International Conference on Robotics and Automation (ICRA)*, pp. 576-581, Alaska, USA, May 2010.
- [16] A. W. Mahoney, D. L. Cowan, K. M. Miller, and J. J. Abbott, "Control of untethered magnetically actuated tools using a rotating permanent magnet in any position," in *Proceedings of the IEEE International Conference on Robotics and Automation (ICRA)*, pp. 3375-3380, Minnesota, USA, May 2012.
- [17] A. W. Mahoney and J. J. Abbott, "Control of untethered magnetically actuated tools with localization uncertainty using a rotating permanent magnet," in *Proceedings of the IEEE RAS/EMBS International Conference on Biomedical Robotics and Biomechanics (BioRob)*, pp. 1632-1637, Rome, Italy, June 2012.
- [18] P. Ryan and E. Diller, "Magnetic actuation for full dexterity micro-robotic control using rotating permanent magnets," *Transactions on Robotics*, vol. 33, no. 6, pp. 1398-1409, December 2017.
- [19] A. W. Mahoney and J. J. Abbott, "Managing magnetic force applied to a magnetic device by a rotating dipole field," *Applied Physics Letters*, vol. 99, September 2011.
- [20] M. E. Alshafeei, A. Hosney, A. Klingner, S. Misra, and I. S. M. Khalil, "Magnetic-Based motion control of a helical robot using two synchronized rotating dipole fields," in *Proceedings of the IEEE RAS/EMBS International Conference on Biomedical Robotics and Biomechanics (BioRob)*, pp. 151-156, São Paulo, Brazil, August 2014.
- [21] A. Hosney, A. Klingner, S. Misra, and I. S. M. Khalil, "Propulsion and steering of helical magnetic microrobots using two synchronized rotating dipole fields in three-dimensional space," in *Proceedings of the IEEE/RSJ International Conference of Robotics and Systems (IROS)*, pp. 1988-1993, Hamburg, Germany, November 2015.
- [22] E. Lauga, "Propulsion in a viscoelastic fluid," *Physics of Fluids*, vol. 19, pp. 083104-1-083104-13, August 2007.
- [23] L. Li and S. E. Spagnolie, "Swimming and pumping by helical waves in viscous and viscoelastic fluids," *Physics of Fluids*, vol. 27, pp. 021902-1-021902-23, February 2015.